Inorg. Chem. **2004**, *43*, 6284–6293

Iron(III) Complexes of Sterically Hindered Tetradentate Monophenolate Ligands as Functional Models for Catechol 1,2-Dioxygenases: The Role of Ligand Stereoelectronic Properties

Marappan Velusamy, Ramasamy Mayilmurugan, and Mallayan Palaniandavar*

Department of Chemistry, Bharathidasan University, Tiruchirapalli 620 024, India

Received February 16, 2004

The iron(III) complexes of the monophenolate ligands 2-(bis(pyrid-2-ylmethyl)aminomethyl)-4-nitrophenol [H(L1)], *N,N*-dimethyl-*N*′-(pyrid-2-ylmethyl)-*N*′-(2-hydroxy-4-nitrobenzyl)ethylenediamine [H(L2)], *N,N*-dimethyl-*N*′-(6-methyl-pyrid-2-ylmethyl)-*N*′-(2-hydroxy-4-nitrobenzyl)ethylenediamine [H(L3)], and *N,N*-dimethyl-*N*′-(1-methylimidazole-2-ylmethyl)-*N*′-(2-hydroxy-4-nitrobenzyl)ethylenediamine [H(L4)] have been obtained and studied as structural and functional models for the intradiol-cleaving catechol dioxygenase enzymes. The complexes $[Fe(L1)Cl_2]\cdot CH_3CN$ (**1**), $[Fe(L2)Cl_2]$ (**2**), $[Fe(L3)Cl_2]$ (**3**), and $[Fe(L4)Cl_2]$ (**4**) have been characterized using absorption spectral and electrochemical methods. The single crystal X-ray crystal structures of **1** and **2** have been successfully determined. Both the complexes possess a rhombically distorted octahedral coordination geometry for the FeN_3OCl_2 chromophore. In **2**, the phenolate oxygen, the pyridine nitrogen, an amine nitrogen, and a chloride ion are located on the corners of a square plane with the nitrogen atom of a $-NMe_2$ group and the other chloride ion occupying the axial positions. In **1**, also the equatorial plane is constituted by the phenolate oxygen, the pyridine nitrogen, an amine nitrogen atom, and a chloride ion; however, the axial positions are occupied by the second pyridine nitrogen and the second chloride ion. Interestingly, the Fe–O–C angle of 136.1° observed for **2** is higher than that (128.5°) in **1**; however, the Fe–O(phenolate) bond distances in both the complexes are the same (1.929 Å). This illustrates the importance of the nearby sterically demanding coordinated $-NMe_2$ group and implies similar stereochemical constraints from the other ligated amino acid moieties in the 3,4-PCD enzymes, the enzyme activity of which is traced to the difference in the equatorial and axial Fe–O(tyrosinate) bonds (Fe–O–C, 133°, 148°). The nature of heterocyclic rings of the ligands and the methyl substituents on them regulates the electronic spectral features, Fe^{III}/Fe^{II} redox potentials, and catechol cleavage activity of the complexes. Upon interacting the complexes with catecholate anions, two catecholate to iron(III) charge transfer bands appear, and the low energy band is similar to that of catechol dioxygenase–substrate complex. Complexes **1** and **3** fail to catalyze the oxidative intradiol cleavage of 3,5-di-*tert*-butylcatechol (H_2DBC). However, interestingly, the replacement of pyridine pendant in **1** by the $-NMe_2$ group to obtain **2** restores the dioxygenase activity, which is consistent with its higher Fe–O–C bond angle. Remarkably, the more basic *N*-methylimidazole ring in **4** facilitates the rate-determining product releasing phase of the catalytic reaction, leading to enhancement in reaction rate and efficient conversion (77.1%) of the substrate to intradiol cleavage products as well. All these observations provide support to the novel substrate activation mechanism proposed for the intradiol-cleavage pathway.

Introduction

The oxidative cleavage of catechol and other dihydroxy aromatic compounds is a key step in the biodegradation of naturally occurring aromatic molecules and many aromatic pollutants in the environment.[1] Catechol 1,2-dioxygenase (CTD) and protocatechuate 3,4-dioxygenase (PCD) are bacterial non-heme iron enzymes,[2,3] which catalyze the

* To whom correspondence should be addressed. E-mail: palani51@sify.com, palanim51@yahoo.com.

(1) (a) Gibson, D. T. *Microbial Degradation of Organic Molecules*; Marcel Dekker: New York, 1984; p 535. (b) Que, L., Jr. In *Bioinorganic Catalysis*, 2nd ed.; Reedijk, J., Bouwman, E., Eds.; Marcel Dekker: New York, 1999; p 269. (c) Kruger, H.-J. In *Biomimetic Oxidations catalyzed by Transition Metal complexes*; Meunier, B., Ed.; Imperial College: London, 2000; p 363.

10.1021/ic049802b CCC: $27.50
Published on Web 09/04/2004

oxidative cleavage of catechols to *cis,cis*-muconic acids with the incorporation of molecular oxygen via a mechanism involving a high-spin ferric center.[4] On the basis of several spectroscopic investigations, the active sites of these enzymes were proposed to consist of a ferric center[4,5] coordinated to two tyrosines, two histidines, and a water molecule. Later, the three-dimensional X-ray crystal structures[6−10] of PCD enzymes have disclosed that in the active site iron(III) is actually liganded by four amino acid residues, namely, Tyr108, Tyr147, His160, and His162 and a solvent molecule to form an approximately trigonal bipyramidal geometry. Very recently, the X-ray crystal structure[11] of a CTD enzyme has also been reported to contain a very similar coordination geometry for iron(III) ligated by two histidine and two tyrosine moieties.

Mimicking these iron−tyrosinate proteins through the synthesis of small molecule active site analogues can provide useful data to improve our understanding of spectra−structure correlations for the protein metal sites. Several iron(III) complexes of tetradentate[12−22] tripodal ligands have been synthesized to mimic the iron(III) coordination environment in the active site. In earlier studies, Que et al. isolated and investigated a series of model complexes[12−15] of the type [FeL(DBC)], where L is a tetradentate tripodal ligand like tris(pyrid-2-ylmethyl)amine (TPA) or nitrilotriacetic acid (NTA) or an NTA analogue with one or two carboxylate pendants and H_2DBC is 3,5-di-*tert*-butylcatechol. These studies have helped in gaining insight into the novel substrate rather than oxygen activation mechanism[2,15,22] of intradiol catechol cleavage. Krebs et al. have used a variety of tripodal ligands with heterocyclic (benz)imidazolyl/pyridyl/quinolyl nitrogen arms to obtain iron(III) model complexes and investigated their dioxygenase activity.[16,17] As the interaction of iron(III) with phenolate moieties of tyrosine residues plays important roles in the enzyme function and in stabilizing the active site geometries of CTD and PCD enzymes, iron(III) complexes of phenolate ligands have attracted much interest as models to mimic the enzyme active sites and function. Two of the tripodal ligand complexes recently reported by Nishida[18] and Que[13,14] to effect oxidative cleavage contain a coordinated phenolate group, in addition to pyridyl moieties. Model compounds synthesized[20,21] by us are derived from both mono- and bis(phenolate) tripodal ligands with pyridine/benzimidazole pendants and were used to cleave the substrate analogue H_2DBC. Very recently, we reported[23] a rare example of a monomeric trigonal bipyramidal iron(III) complex derived from a tripodal sterically hindered bis(phenolate) ligand; the incorporation of electron-releasing 2,4-dimethyl groups on the phenolate moieties confers the lower coordination number for iron(III). However, interestingly, the complex failed to show any intradiol cleavage of catechol. On the other hand, the other five-coordinate complex[24] reported by Fujii et al. owes its unusual geometry to the steric bulk of the bis(phenolate) Schiff base ligand. These observations prompted us to design new sterically hindered phenolate ligands to closely mimic the enzyme active site structure and function. In the present report are described the results of our study on the structure, spectra, and redox properties of iron(III) complexes of the three new tripodal monophenolate ligands H(L2)−H(L4) (Scheme 1) containing the sterically demanding $-NMe_2$ group as well as the pendant (6-methyl)pyridine or *N*-methyl-

Scheme 1. Structures of the Tripodal Ligands Employed in the Study

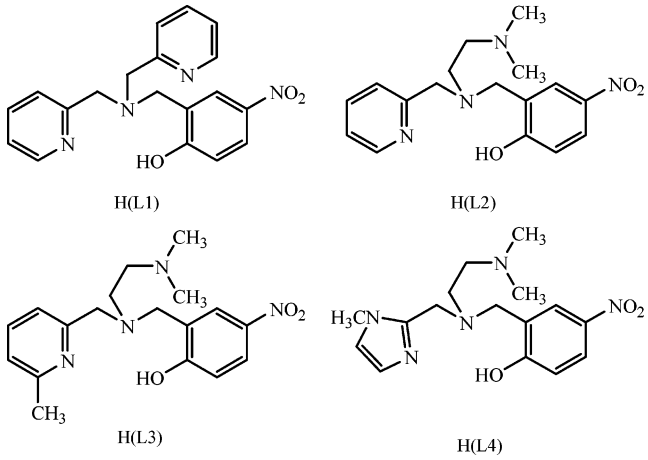

(2) Lipscomb, J. D.; Orville, A. M. *Met. Ions Biol. Syst.* **1992**, *28*, 243.
(3) (a) Bugg, T. D. H.; Winfield, C. J. *Nat. Prod. Rep.* **1998**, *15*, 513. (c) Feig, A. L.; Lippard, S. J. *Chem. Rev.* **1994**, *94*, 759.
(4) Que, L., Jr. *Struct. Bonding (Berlin)* **1980**, *40*, 39. (b) Que, L., Jr. *Adv. Inorg. Biochem.* **1983**, *5*, 167. (c) Que, L., Jr.; Reynolds, M. F. *Met. Ions Biol. Syst.* **2000**, *37*, 505.
(5) (a) Whittaker, J. W.; Lipscomb, J. D. *J. Biol. Chem.* **1984**, *259*, 4487. (b) Que, L., Jr. In *Iron Carriers and Iron Proteins*; Loehr, T. M., Ed.; VCH: New York, 1989; pp 467−524.
(6) Ohlendorf, D. H.; Lipscomb, J. D.; Weber, P. C. *Nature* **1988**, *336*, 403.
(7) Ohlendorf, D. H.; Orville, A. M.; Lipscomb, J. D. *J. Mol. Biol.* **1994**, *244*, 586.
(8) Vetting, M. W.; Earhart, C. A.; Ohlendorf, D. H. *J. Mol. Biol.* **1994**, *236*, 372.
(9) Frazee, R. W.; Orville, A. M.; Dolbeare, K. B.; Yu, H.; Ohlendorf, D. H.; Lipscomb, J. D. *Biochemistry* **1998**, *37*, 2131.
(10) Vetting, M. W.; D'Argenio, D. A.; Ornston, L. N.; Ohlendorf, D. H. *Biochemistry* **2000**, *39*, 7943.
(11) Vetting, M. W.; Ohlendorf, D. H. *Structure* **2000**, *8*, 429.
(12) Cox, D. D.; Que, L., Jr. *J. Am. Chem. Soc.* **1988**, *110*, 8085.
(13) Que, L., Jr.; Kolanczyk, R. C.; White, L. S. *J. Am. Chem. Soc.* **1987**, *109*, 5373.
(14) Cox, D. D.; Benkovic, S. J.; Bloom, L. M.; Bradley, F. C.; Nelson, M. J.; Que, L., Jr.; Wallick, D. E. *J. Am. Chem. Soc.* **1988**, *110*, 2026.
(15) Jang, H. G.; Cox, D. D.; Que, L., Jr. *J. Am. Chem. Soc.* **1991**, *113*, 9200.
(16) (a) Pascaly, M.; Duda, M.; Rompel, A.; Sift, B. H.; Klaucke, W. M.; Krebs, B. *Inorg. Chim. Acta* **1999**, *291*, 289. (b) Pascaly, M.; Nazikkol, C.; Scweppe, F.; Wiedeman, A.; Zurlinden, K.; Krebs, B. *Z. Anorg. Allg. Chem.* **2000**, *626*, 50. (c) Pascaly, M.; Duda, M.; Schweppe, F.; Zurlinden, F.; Muller, K.; Krebs, B. *J. Chem. Soc., Dalton Trans.* **2001**, 828.
(17) Merkel, M.; Müller, F. K.; Krebs, B. *Inorg. Chim. Acta* **2002**, *337*, 308.
(18) Nishida, Y. Shimo, H.; Kida, S. *J. Chem. Soc., Chem. Commun*. **1984**, 1611.
(19) (a) Nishida, Y.; Takahashi, S. *J. Chem. Soc., Dalton Trans.* **1988**, 691. (b) Ito, S.; Suzuki, M.; Kobayashi, T.; Itoh, H.; Harada, A.; Ohba, S.; Nishida, Y. *J. Chem. Soc., Dalton Trans.* **1996**, 2579. (c) Ito, S.; Ishikawa, Y.; Nishino, S.; Kobayashi, T.; Ohba, S.; Nishida, Y. *Polyhedron* **1998**, *17*, 4379.
(20) Viswanathan, R.; Palaniandavar, M.; Balasubramanian, T.; Muthiah, T. P. *Inorg. Chem.* **1998**, *37*, 2943.
(21) Viswanathan, R.; Palaniandavar, M. *Proc. Indian Acad. Sci., Chem. Sci.* **1996**, *108*, 235.
(22) Que, L., Jr.; Ho, R. Y. N. *Chem. Rev.* **1996**, *96*, 2607.
(23) Velusamy, M.; Palaniandavar, M.; Srinivasagopalan, R.; Kulkarni, G. U. *Inorg. Chem.* **2003**, *37*, 2943.
(24) Fujii, H.; Funabashi, Y. *Angew. Chem., Int. Ed*. **2002**, *41*, 3638.

Scheme 2. Structures of the Catechol Derivatives Used in This Work

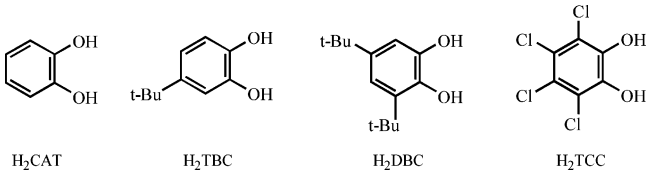

imidazole nitrogen to mimic the imidazole donor function of the enzymes.

The steric and electronic influence of the ligand nitrogen donor set on the spectral and redox behavior and the dioxygenase activity of the complexes is probed in this work. The X-ray crystal structure of one of the new complexes has been determined to demonstrate the availability of two *cis* coordination sites for adduct formation by substrate molecules. All the complexes have been interacted with a series of catechols (Scheme 2); only a few studies[16] have been devoted to understand the effect of variation in catechols. The advantages of using H_2DBC as substrate are the relatively high stability of the main cleavage product and the fast reaction of the catecholate complexes with dioxygen.

Experimental Section

Materials. Synthesis of Ligands. 2-(Bis(pyrid-2-ylmethyl)-aminomethyl)-4-nitrophenol [H(L1)]. This was synthesized employing the previously published procedure.[20]

***N,N*-Dimethyl-*N*′-(pyrid-2-ylmethyl)-*N*′-(2-hydroxy-4-nitrobenzyl)ethylenediamine H(L2).** This ligand was synthesized in two steps. The first step in the synthesis was the preparation of *N,N*-dimethyl-*N*′-(pyrid-2-ylmethyl)ethylenediamine, which was then reacted with 2-hydroxy-5-nitrobenzyl chloride in the second step to obtain the ligand **H(L2)**.

Step 1. Synthesis of *N,N*-Dimethyl-*N*′-(pyrid-2-ylmethyl)-ethylenediamine. *N,N*-Dimethyl-*N*′-(pyrid-2-ylmethyl)ethylenediamine was prepared as reported elsewhere. ^{1}H NMR (200 MHz, $CDCl_3$) δ 2.20 (s, $N(CH_3)_2$), 2.4 (t, CH_2), 2.7 (t, CH_2), 3.90 (s, py-CH_2), 3.0 (sb, NH) 7.1−8.5 (pyH).

Step 2. Synthesis of H(L2). To *N,N*-dimethyl-*N*′-(pyrid-2-ylmethyl)ethylenediamine (0.36 g, 2 mmol) in methanol (20 mL) was added triethylamine (0.2 g, 2 mmol) followed by 2-hydroxy-5-nitrobenzyl chloride (0.38 g, 2 mmol) in methanol. This mixture was refluxed for 2 h and rotary evaporated to dryness. To this was added excess THF, and the mixture was then cooled. The Et_3N·HCl salt formed was filtered off, and the filtrate was rotary evaporated to dryness to get the ligand 2-(bis(pyrid-2-ylmethyl)-aminomethyl)-4-nitrophenol as an yellow oil. The oil was chromatographed with CH_2Cl_2−MeOH solvent mixture (5:1).

***N,N*-Dimethyl-*N*′-(6-methylpyrid-2-ylmethyl)-*N*′-(2-hydroxy-4-nitrobenzyl)-ethylenediamine H(L3).** The ligand was synthesized in two steps using the procedure employed for H(L2) but using 6-methyl-2-pyridinecarboxaldehyde instead of pyridine-2-carboxaldehyde. The first step in the synthesis was the preparation of *N,N*-dimethyl-*N*′-(6-methylpyrid-2-ylmethyl)ethylenediamine, which was then reacted with 2-hydroxy-5-nitrobenzyl chloride in the second step.

***N,N*-Dimethyl-*N*′-(1-methylimidazole-2-ylmethyl)-*N*′-(2-hydroxy-4-nitrobenzyl)-ethylenediamine H(L4).** This ligand was also prepared in two steps. The first step in the synthesis was the preparation of *N,N*-dimethyl-*N*′-(1-methylimidazole-2-ylmethyl)-ethylenediamine, which was then reacted with 2-hydroxy-5-nitrobenzyl chloride in the second step.

The ligand *N,N*-dimethyl-*N*′-(1-methylimidazole-2-ylmethyl)-ethylenediamine was prepared by the same method as that used for *N,N*-dimethyl-*N*′-(pyrid-2-ylmethyl)ethylenediamine except that 1-methyl-2-imidazolecarboxaldehyde was used instead of pyridine-2-carboxaldehyde. The yield was 60%. ^{1}H NMR (200 MHz, $CDCl_3$) δ 3.8 (s, Im-CH_3), 2.3 (t, CH_2), 2.7 (t, CH_2), 3.86 (s, py-CH_2), 2.2 (s, 6H, $N(CH_3)_2$), 6.82 (d, 1H, im), 6.92 (d, 1H, im).

To *N,N*-dimethyl-*N*′-(1-methylimidazole-2-ylmethyl)ethylenediamine (0.37 g, 2 mmol) in methanol (20 mL) was added triethylamine (0.2 g, 2 mmol) followed by 2-hydroxy-5-nitrobenzyl chloride (0.38 g, 2 mmol) in methanol. This mixture was refluxed for 2 h and rotary evaporated to dryness. To this was added excess THF, and then the mixture was cooled. The Et_3N·HCl salt formed was filtered off, and the resulting solution was rotary evaporated to dryness to get the ligand 2-(bis(pyrid-2-ylmethyl)aminomethyl)-4-nitrophenol as an yellow oil. The resulting oil was dissolved in methanol and used as such for preparation of complex without further purification.

Synthesis of Complexes. The complex $[Fe(L1)Cl_2]$ (**1**) was prepared as reported already. All the other complexes were prepared by adding an equivalent amount of a solution of anhydrous ferric chloride in methanol to a methanol solution of the ligand in the presence of an equivalent amount of triethylamine; the latter was needed to abstract the phenolic hydrogen of the ligand. The solution was then stirred for an hour to obtain a violet precipitate, which was filtered off, washed with small amounts of cold methanol, and dried in vacuo over P_4O_{10}. Anal. Calcd for $C_{17}H_{21}N_4O_3FeCl_2$ ([Fe(L2)Cl_2], **2**): C, 44.77; H, 4.64; N, 12.28. Found: C, 44.75; H, 4.60; N, 12.30. Calcd for $C_{18}H_{23}N_4O_3FeCl_2$ ([Fe(L3)Cl_2], **3**): C, 45.98; H, 4.93; N, 11.92. Found: C, 45.60; H, 4.95; N, 11.90. Calcd for $C_{16}H_{22}N_5O_3FeCl_2$ ([Fe(L4)Cl_2], **4**): C, 41.86; H, 4.83; N, 15.25. Found: C, 41.85; H, 4.80; N, 15.25%.

X-ray quality crystals of $[Fe(L1)Cl_2]$·CH_3CN (**1**) were obtained by slow evaporation of an CH_3CN solution of the complex [Fe(L1)Cl_2], and those of $[Fe(L2)Cl_2]$ (**2**) were obtained by vapor diffusion of diethyl ether into an CH_3CN solution of the complex.

Crystallographic Data Collection and Structure Analysis. The crystal data[25] for $[Fe(L1)Cl_2]$·CH_3CN (**1**) were collected on an Enraf-Nonius CAD4 diffractometer using Mo Kα radiation (50 kV, 40 mA) at 293(2) K, and the crystal data[26] for $[Fe(L2)Cl_2]$ were collected on a Siemens three-circle diffractometer attached with CCD area detector using Mo Kα radiation. The unit cell parameters and the orientation matrix of the $[Fe(L2)Cl_2]$ (**2**) crystal were

(25) The crystal structure of this complex has been reported already by Nishida et al.: Ito, S.; Suzuki, M.; Kobayashi, T.; Itoh, H.; Harada, A.; Ohba, S.; Nishida, Y. *J. Chem. Soc., Dalton Trans.* **1996**, 2579. However, the present structure is more accurate. Crystal data for [Fe(L1)Cl_2]·CH_3CN at 293(2) K: empirical formula $C_{21}H_{20}N_5O_3FeCl_2$, formula weight 517.17, triclinic, space group $P\bar{1}$, a = 7.027(3) Å, b = 11.951(2) Å, c = 13.746(2) Å, α = 88.86(1)°, β = 81.40(2)°, γ = 79.43(2)°. V = 1121.9(5) Å^3, Z = 2, ρ(calcd) = 1.699 g/cm^3, absorption coefficient, 1.631 mm^{-1}, θ range for data collection 2.28−24.97°, index ranges $0 \le h \le 8$, $-13 \le k \le 14$, $-16 \le l \le 16$, refinement method full-matrix least-squares on F^2, data/restraints/parameters 3940/0/292, GOF on F^2 1.134, final R indices [$I > 2\sigma(I)$], R1 = 0.0368, wR2 = 0.0961, R indices (all data), R1 = 0.0674, wR2 = 0.1630.

(26) Crystal data for $[Fe(L2)Cl_2]$ at 293(2) K: empirical formula $C_{17}H_{21}N_4O_3FeCl_2$, formula weight 456.13, triclinic, space group *Pccn*, a = 38.032(8) Å, b = 8.047(2) Å, c = 12.809(3) Å, α = 90.00°, β = 90.00°, γ = 90.00°. V = 3920.10(14?) Å^3, Z = 8, ρ(calcd) = 1.546 g/cm^3, absorption coefficient, 1.631 mm^{-1}, θ range for data collection 2.61−24.97°, index ranges $0 \le h \le 8$, $-9 \le k \le 9$, $-14 \le l \le 14$, refinement method full-matrix least-squares on F^2, data/restraints/parameters 2904/0/248, GOF on F^2 0.823, final R indices [$I > 2\sigma(I)$], R1 = 0.0695, wR2 = 0.1690, R indices (all data), R1 = 0.0674, wR2 = 0.1630.

Table 1. Selected Bond Lengths [Å] and Bond Angles [deg] for $[Fe(L2)Cl_2]$

Fe(1)−O(1)	1.929(5)
Fe(1)−N(1)	2.180(7)
Fe(1)−N(2)	2.213(7)
Fe(1)−Cl(1)	2.285(3)
Fe(1)−N(3)	2.334(7)
Fe(1)−Cl(2)	2.339(2)
O(1)−Fe(1)−N(1)	164.2(3)
O(1)−Fe(1)−N(2)	87.0(2)
N(1)−Fe(1)−N(2)	77.3(3)
O(1)−Fe(1)−Cl(1)	99.8(2)
N(1)−Fe(1)−Cl(1)	95.1(2)
N(2)−Fe(1)−Cl(1)	165.33(19)
O(1)−Fe(1)−N(3)	91.7(3)
N(1)−Fe(1)−N(3)	83.5(3)
N(2)−Fe(1)−N(3)	78.5(3)
Cl(1)−Fe(1)−N(3)	88.3(2)
O(1)−Fe(1)−Cl(2)	95.20(18)
N(1)−Fe(1)−Cl(2)	87.79(18)
N(2)−Fe(1)−Cl(2)	94.04(18)
Cl(1)−Fe(1)−Cl(2)	98.23(10)
N(3)−Fe(1)−Cl(2)	169.5(2)

initially determined using 60 reflections from 25 frames collected over a small ω scan. A hemisphere of reciprocal space was then collected using SMART software[27] with the 2θ setting at 28°. Data reduction was performed using the SAINT program, and the orientation matrix along with the detector and the cell parameters were refined for every 40 frames on all the measured reflections. The intensity data were corrected for Lorentz and polarization effects, a semiempirical absorption correction was carried out using SADABS[28] for **2**, and an empirical absorption correction based on an ω scan was applied for **1** using the MolEN program.[29] The structures were solved by a direct method using the SHELXS 97 program[30] and refined by full-matrix least-squares method of F^2 using the SHELXL 97 program.[31] All the non-hydrogen atoms were refined anisotropically. Hydrogen atoms were geometrically fixed at their calculated positions. The molecular structure was drawn using ORTEP.[32] The selected bond lengths and bond angles for **2** are given in Table 1. The structure of **1**·CH_3CN (Figure S1), the final atomic coordinates of non-hydrogen atoms, a complete set of bond lengths and bond angles, anisotropic thermal parameters for non-hydrogen atoms, and atomic coordinates for hydrogen atoms are given in the Supporting Information.

Reactivity Studies. The catechol-cleaving dioxygenase activity of the complexes toward 3,5-di-*tert*-butylcatechol (H_2DBC) was examined[17,23,33] by exposing, to dioxygen, a solution of the iron(III) complex−DBC^{2-} adduct generated in situ by treating the complex (2.3×10^{-4} M) with H_2DBC (2.3×10^{-4} M) and piperidine (4.6×10^{-4} M). Kinetic analyses[33,34] of the catechol cleavage reactions were carried out by time-dependent measurement of the disappearance of the lower energy catecholate to iron(III) LMCT band at ambient temperature (25 °C). The solubility[35] of O_2 in DMF at 25 °C was taken as 4.86 mM.

The dioxygenase activities of the present complexes were determined using a known[36,37] procedure with modifications. The complex (0.15 mmol), 3,5-di-*tert*-butylcatechol (0.034 g, 0.15 mmol), and piperidine (0.208 mmol) were dissolved in DMF (10 mL) at 1 atm oxygen. After 48 h, the reaction was quenched by the addition of 6 M HCl solution (30 mL). The products were extracted from the aqueous DMF solution with $CHCl_3$ (3×50 mL). The clear yellow $CHCl_3$ layer was separated, washed twice, first with 2 M HCl (20 mL) and then with water, and then extracted with a saturated $NaHCO_3$ solution (10 mL) to separate the acid products. The $CHCl_3$ layer was saved for further manipulation for obtaining nonacid products. The aqueous solution was acidified with 6 M HCl and then extracted twice with 5 mL of $CHCl_3$. The $CHCl_3$ extracts were combined, dried over anhydrous Na_2SO_4, and filtered and the solvent rotary evaporated to yield no acid product. The $CHCl_3$ layer remaining after $NaHCO_3$ extraction was dried over 5 g of anhydrous Na_2SO_4 for 8 h at room temperature. The Na_2SO_4 was then filtered off and rinsed twice with 5 mL of fresh $CHCl_3$, and the combined filtrate was evaporated in vacuo at 40 °C, which yields nonacid products (**2**, 0.030 g; **4**, 0.028 g). Further purification of the products was accomplished by column chromatography using silica gel and 200 mL of $CHCl_3$ as eluent. The products were analyzed as a mixture using H_2DBC substrate as standard under identical conditions and an HP 6890 GC series gas chromatograph equipped with a FID detector and an HP-5 capillary column (30 m $\times$ 0.32 mm $\times$ 2.5 μm) with the following temperature program: initial temperature, 50 °C; heating rate, 5 °C min^{-1}; final temperature, 250 °C; injector temperature, 150 °C; and FID temperature, 280 °C. GC-MS analysis was performed on a Perkin-Elmer Clarus 500 GC-MS instrument using a PE-5 (HP-5 equivalent) capillary column under conditions identical to those used for GC analysis.

Results and Discussion

The present ligands were synthesized according to known procedures,[38] which involve simple substitution reactions. They may be regarded as derivatives of the exclusively pyridine containing ligand TPA. The pendant pyridine/imidazole functionality has been incorporated into the ligand to provide a systematic variation in the Lewis acidity of the iron(III) center. The bulky *N*,*N*-dimethyl group, the pyridine ring nitrogen sterically hindered by a 6-methyl group, and the more basic *N*-methyl-imidazole moiety [pK_a (BH^+): imidazole, 6.0; pyridine, 5.2] in the ligands are expected to influence the iron(III) coordination structures as well as the electronic properties of the complexes and offer steric hindrance to the substrates so as to closely approximate the active site in enzyme−substrate complexes. For comparison, we isolated the already reported[20] complex **1** but as its CH_3CN solvate, **1**·CH_3CN. In these complexes, the NO_2 group has been introduced because of the ease of synthesis

(27) Siemens Analytical X-ray Instruments Inc., Madison, WI, 1995.
(28) Sheldrick, G. M. *SADABS User Guide*; University of Göttingen: Göttingen, Germany, 1997.
(29) Rontgenweg, B. V. *MolEN Structure Determination System*; Delft Instruments, X-ray diffraction: 1:2644 BD Delft, The Netherlands, 1990.
(30) Sheldrick, G. M. *SHELXS-97: Program for the Solution of Crystal Structure*; University of Göttingen: Göttingen, Germany, 1997.
(31) Sheldrick, G. M. *SHELXS-97: Program for the Refinement of Crystal Structure*; University of Göttingen: Göttingen, Germany, 1997.
(32) Zsolnai, L. *ZORTEP, An interactive ORTEP program*; University of Heidelberg: Heidelberg, Germany, 1996.
(33) (a) Mialane, P.; Tehertanov, L.; Banse, F.; Sainton, J.; Girerd, J. *Inorg. Chem.* **2000**, *39*, 2440. (b) Mialane, P.; Anxolabéhère-Mallart, E.; Blondin, G.; Nivorojkine, A.; Guilhem, J.; Tchertanova, L.; Cesario, M.; Ravi, N.; Bominaar, E.; Girerd, J.-J.; Münck, E. *Inorg. Chim. Acta* **1997**, *263*, 367.
(34) Yamahara, R.; Ogo, S.; Watanabe, Y.; Funabiki, T.; Jitsukawa, K.; Masuda, H.; Einaga, H. *Inorg. Chim. Acta* **2000**, *300*, 587.
(35) *Kagaku-Binran Basic Part II*, 2nd ed.; Japan Chemical Society: Tokyo, Japan, 1975.
(36) Funabiki, T.; Mizoguchi, A.; Sugimoto, T.; Tada, S.; Tsuji, M.; Sakamoto, H.; Yoshida, S. *J. Am. Chem. Soc.* **1986**, *108*, 2921.
(37) Weiner, H.; Hayashi, Y.; Finke, R. G. *Inorg. Chim. Acta* **1999**, *291*, 426.
(38) Wong, Y.-L.; Yan, Y.; Chan, E. S. H.; Yang, Q.; Mak, T. C. W.; Ng, D. K. P. *J. Chem. Soc., Dalton Trans.* **1998**, 3057.

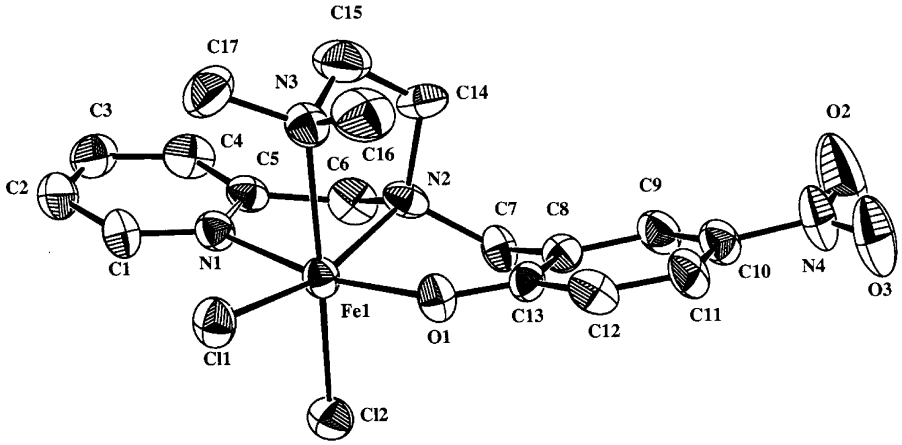

Figure 1. ORTEP drawing of $[Fe(L2)Cl_2]$ (**2**) showing the atom numbering scheme and the thermal motion ellipsoids (50% probability level) for the non-hydrogen atoms.

from the synthetically readily achievable benzyl chloride and also because of its use in studying the factors affecting the spectral and redox properties of the iron(III) complexes. The tetradentate ligands provide a reasonable analogue to histidine and tyrosinate coordination in CTD and PCD enzymes via the heterocyclic nitrogen donors and phenolate moieties, respectively. Further, as the catecholate adducts isolated yielded unsatisfactory analytical results, they were generated in solution for spectral studies.

On the basis of the results of elemental analysis and the crystal structures of **1**·CH_3CN and **2** (Figure 1) and evidence from spectral studies, the structures of all the present complexes may be assigned as distorted octahedral. Conductivity studies (Λ_M, 150−205 ohm^{-1} cm^2 mol^{-1}) reveal that the chloride ions are not at all coordinated in methanol solution. All the iron(III) complexes have magnetic moments in the range 5.3−5.5 μ_B at room temperature, which is consistent with a high-spin ferric center.

Description of the X-ray Crystal Structure of [Fe(L2)-Cl_2] (2). The structure of molecule **2** is shown in Figure 1 together with the atom numbering scheme. The complex molecule has an FeN_3OCl_2 coordination sphere with a distorted octahedral geometry, constituted by three nitrogen atoms and one phenolate oxygen atom from the tripodal ligand and two chloride ions. The Fe−N_{py} bond length (2.180 Å) is shorter than the Fe−N_{amine} bond distances (Fe−N2, 2.213 Å; Fe−N3, 2.334 Å), which is expected of the difference in hybridization of the nitrogen atoms. The Fe−N_{amine} bond distances are similar to the octahedral Fe(III)−N bond distance[17,20,21,23,39−46] of ∼2.15 Å. Further, the Fe−N3 bond is significantly longer than the Fe−N2 bond due to the inability of the sterically hindering $-N(CH_3)_2$ group to properly orient itself toward iron(III). The deviation from a perfect octahedral coordination geometry is best illustrated by the N3−Fe1−Cl2 (169.5°) and O1−Fe1−N1 (164.2°) bond angles, which markedly deviate from that (180°) of an ideal octahedron. The bond distance of Fe−Cl1 (2.285 Å) is in the same range as those for octahedral iron(III) complexes[17,20,21,23,45] but is significantly shorter than Fe−Cl2 (2.339 Å) suggesting that the Cl2 ligand is more labile than the other. Such electronic structure differences between the *cis* chloride ions would encourage asymmetric bidentate coordination of the catecholate substrates, which is essential for substrate activation, subsequent reaction with molecular oxygen, and removal. This is relevant to the 4-HBA-PCD complex[47,48] (4-HBA = 4-hydroxybenzoate) in which a doubly deprotonated form of 4-HBA is chelated. The observed Fe−O1 distance (1.929 Å) is shorter than the average octahedral Fe^{III}−O distance[20,21,23,39−46,49,50] of ∼1.98 Å suggesting strong iron−oxygen overlap.[45] The phenolate oxygen in the six-membered chelate ring has an Fe−O1−C13 bond angle of 136.1°, which is higher than the ideal value of 120° for an sp^2 hybridized[32] phenolate oxygen atom indicating that the latter (in-plane pπ orbital) interacts[45] less strongly with a half-filled dπ* orbital on iron(III). Also, the angle is higher than the average Fe−O−C bond angle of ∼128.5° observed in other octahedral iron(III)−phenolate complexes.[20,21,23,39−45]

A comparison of the structural parameters of **2** with those of **1**·CH_3CN reveals remarkable differences in their structures. The replacement of one of the pyridine pendants in **1**·CH_3CN by the sterically demanding $-NMe_2$ group to obtain **2** results in shortening of Fe−N but elongation of Fe−Cl bonds. Theoretical calculations[50] show that as the Fe−

(39) Lauffer, R. B.; Heistand, R. H., II; Que, L., Jr. *Inorg. Chem.* **1983**, *22*, 50.
(40) Ainscough, E. W.; Brodie, A.; Plowman, J. E.; Brown, K. L.; Addison, A. W.; Gaisford, A. R. *Inorg. Chem.* **1980**, *19*, 3655.
(41) Davis, J. C.; Kung, W. S.; Averill, B. *Inorg. Chem.* **1986**, *25*, 394.
(42) Yan, S.; Que, L., Jr.; Taylor, L. F.; Anderson, O. P. *J. Am. Chem. Soc.* **1988**, *110*, 5222.
(43) Clarke, E. T.; Martell, A. E.; Reibenspies, J. *Inorg. Chim. Acta* **1992**, *196*, 177.
(44) Malfant, I.; Margenstern-Badarau, I.; Philoche-Laviselles, M.; Lloret, F. *J. Chem. Soc., Chem. Commun.* **1990**, 1338.
(45) McDevitt, M. R.; Addison, A. W.; Sinn, E.; Thomson, L. K. *Inorg. Chem.* **1980**, *19*, 3655.
(46) Okamoto, K.-L.; Kanamori, K.; Hidaka, J. *Acta Crystallogr.* **1990**, *C46*, 1640.
(47) Whittaker, J. W.; Lipscomb, J. D.; Kent, T. A.; Munck, E. *J. Biol. Chem.* **1984**, *259*, 4466.
(48) Orville, A. M.; Lipscomb, J. D. *J. Biol. Chem.* **1989**, *264*, 8791.
(49) (a) Shyu, H. L.; Wei, H. H.; Lee, G. H.; Wang, Y. *J. Chem. Soc., Dalton Trans.* **2000**, 915. (b) Lubben, M.; Meetsman, A.; Bolhuis, F.; Feringa, B. L. *Inorg. Chim. Acta* **1994**, *215*, 123. (c) Setyawati, I.; Rettig, S. J.; Orvig, C. *Can. J. Chem.* **1999**, *77*, 2033.
(50) Davies, M. I.; Orville, A. M.; Neese, F.; Zaleski, J. M.; Lipscomb, J. D.; Solomon, E. I. *J. Am. Chem. Soc.* **2002**, *124*, 602.

Table 2. Electronic Spectral Data[a] for Iron(III) Complexes and Their Adducts in Acetonitrile Solution

added ligand	λ_{max}, nm (ϵ, M^{-1} cm^{-1})			
	[Fe(L1)Cl_2]	[Fe(L2)Cl_2]	[Fe(L3)Cl_2]	[Fe(L4)Cl_2]
none	540 (3200)	545 (3755)	550 (3190)	535 (3570)
	435 (2325)	430 (3195)	365 (13 890)	425 (3645)
	365 (17 850)	360 (17 405)	265 (11 130)	360 (18 090)
	250 (14 930)	250 (14 035)		290 (7645)
CAT^{2-}	725 (2885)	730 (2670)	740 (3035)	710 (2425)
	480 (2960)	480 (3025)	480 (3205)	485 (2760)
	365 (14 740)	365 (14 695)	370 (13 670)	375 (15 380)
	290 (8620)	295 (8920)	290 (9065)	295 (8695)
TBC^{2-}	755 (2935)	760 (2825)	780 (3365)	740 (2545)
	485 (3200)	485 (3376)	485 (3465)	490 (3060)
	370 (15700)	370 (14 798)	370 (14 025)	375 (15 450)
	290 (9030)	295 (9345)	295 (9475)	295 (8990)
DBC^{2-}	780 (3570)	790 (3260)	800 (3465)	760 (2630)
	490 (3325)	485 (3320)	495 (3265)	490 (3085)
	375 (15 525)	380 (14 770)	380 (14 040)	385 (15 090)
	290 (8585)	295 (8795)	290 (8910)	290 (8280)
TCC^{2-}	650 (3795)	650 (3365)	665 (3650)	635 (3175)
	490 (3675)	480 (3755)	485 (3820)	490 (3570)
	360 (15 050)	355 (15 570)	350 (14 630)	360 (15 585)
	310 (10 115)	310 (10 575)	310 (10 060)	310 (9370)

[a] Concentration of iron(III) complexes, 2×10^{-4} M. The ratio of added ligands to iron(III) complexes, 1:1. The anions were generated by adding 2 equiv of triethylamine. H_2DBC = 3,5-di-*tert*-butylcatechol, H_2TBC = 4-*tert*-butylcatechol, H_2CAT = catechol, H_2TCC = tetrachlorocatechol.

O−C bond angle increases the phenolate donor becomes less donating to interact weakly with iron. But, interestingly, though the Fe−O−C bond angle in **2** is higher than that (128.5°) in **1**·CH_3CN, the Fe−O bond distance is the same (1.928 Å) for both the complexes. The replacement of the pyridine moiety in **1**·CH_3CN by the sterically demanding $-NMe_2$ group enhances the Fe−O−C bond angle but decreases the Fe−O−C−C dihedral angle from 59.0° to 15.2°. This enhances the π-back-bonding, which involves the dπ orbitals of iron and the relatively low lying π^* orbital (vs phenolate ion)[21] of the weakly σ-bonding *p*-nitrophenolate, leading to a stronger Fe−O bond. Similar higher Fe−O−C bond angles (135.3°, 135.6°) but varying Fe−O bond lengths (1.890, 1.993 Å) observed for [Fe(L5)Cl] (**5**) [H_2(L5) = *N*,*N*-dimethyl-*N*,*N*-bis(2-hydroxy-5-nitrobenzyl)ethylenediamine] are consistent with the lower Fe−O−C−C dihedral angles (13.08°, 13.15°).[23] However, for the analogous bis-(2,4-dimethylphenolate)iron(III) complex,[23] also containing the coordinated $-NMe_2$ group, only a lower Fe−O−C (122.05°, 122.15°) but higher Fe−O−C−C dihedral angle (31.30°, 55.97°) were observed revealing a weaker 2,4-dimethylphenolate−iron(III) π-interaction. This illustrates the importance of extended π-delocalization involving *p*-nitrophenolate and iron(III) d-orbitals.

Electronic Absorption Spectra. The results of electronic absorption spectral studies on the complexes and their adducts with different substituted catechols are collected in Table 2. The main feature of the electronic spectra (Figure 2) of the iron(III) phenolate complexes is the relatively intense band in the 535−545 nm region, which is assigned to phenolate (π) → Fe(III) (dπ^*) ligand to metal charge-transfer (LMCT) transition.[50,51] On the other hand, the high energy band observed in the 425−435 nm range is assigned[50] to a phenolate (σ) → Fe(III) ($d_{x^2-y^2}/d_{z^2}$) ligand to metal charge-transfer transition. While the intense absorption

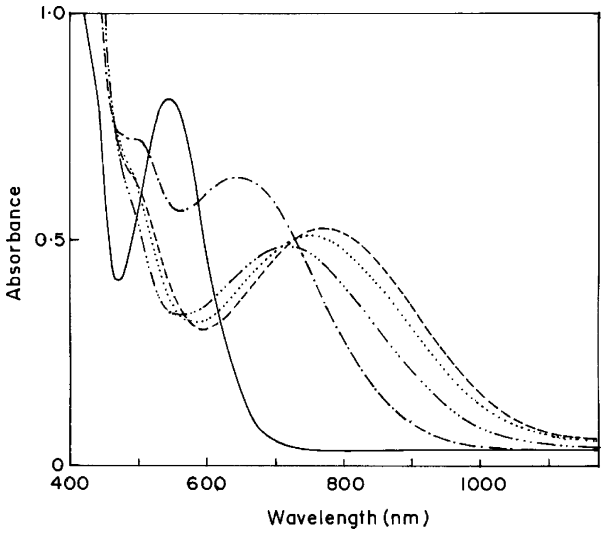

Figure 2. Electronic absorption spectra of [Fe(L4)Cl_2] (**4**) (2×10^{-4} M) and its catecholate adducts generated in situ by adding equimolar amounts of differently substituted catecholate anions in acetonitrile solution: [Fe(L4)Cl_2] (—), [Fe(L4)(TCC)]$^+$]$^+$ (-·-), [Fe(L4)(CAT)]$^+$(-···-), [Fe(L4)(TBC)]$^+$ (····), [Fe(L4)(DBC)]$^+$ (- - -).

maximum in the 360−365 nm range is caused by a $\pi \rightarrow \pi^*$ transition involving a *p*-nitrophenolate[17,52] moiety, the intense absorption band observed near 255 nm is due to the $\pi \rightarrow \pi^*$ transition within the pyridine/imidazole/phenolate moiety. The band energy of the lowest energy LMCT band decreases in the order **4** > **2** > **1** > **3**, reflecting the increase in Lewis acidity of the iron(III) center in this order. On replacing the py moiety in **1** by the less strongly binding and sterically hindering $-NMe_2$ group as in **2** (cf. above), the Lewis acidity increases. The negative charge built[14] on iron(III) on replacing the py moiety in **2** by the more basic *N*-methylimidazole moiety to obtain **4** raises the iron d-orbital energy, leading to the higher LMCT band energy for **4**. Similarly, the incorporation of the sterically demanding 6-Me group in **2** to obtain **3** would hinder the coordination of py nitrogen leading to a decrease in negative charge built on iron(III) and hence the lower LMCT band energy for **3**. Thus, the Lewis acidity of the iron(III) center is fine-tuned by modifying the ligand environment through the replacement of the py moiety by imidazole moiety and suitable incorporation of methyl groups on the heterocyclic rings.

Two new visible bands (480−490, 635−800 nm, Table 2, Figure 2), which appear on adding catecholate dianions, are assignable to a catecholate-to-Fe(III) LMCT transition[53] involving two different catecholate orbitals on the chelated catecholate. The position of the low rather than high energy LMCT band of the catecholate adducts shows remarkable

(51) (a) Casella, L.; Gullotti, M.; Pintar, A.; Messouri, L.; Rockenbauer, A.; Gyor, M. *Inorg. Chem.* **1987**, *26*, 1031. (b) Wang, S.; Wang, L.; Wang, X. Luo, Q. *Inorg. Chim. Acta* **1997**, *254*, 71. (c) Krebs, B.; Schepers, K.; Bremer, B.; Henkel, G.; Althus, E.; Muller-Warmuth, W.; Griesar, K.; Haase, W. *Inorg. Chem.* **1996**, *35*, 2360.
(52) Molenveld, P.; Engbersen, J. F. J.; Kooijman, H.; Spek, A. L.; Reinhoudt, D. N. *J. Am. Chem. Soc.* **1998**, *120*, 6726.
(53) (a) Cox, D. D.; Que, L., Jr. *J. Am. Chem. Soc.* **1988**, *110*, 8085. (b) Salama, S.; Stong, J. D.; Neilands, J. B.; Spiro, T. G.; *Biochemistry* **1978**, *17*, 3781. (c) Koch, W.; Kruger, H.-J. *Angew. Chem., Int. Ed. Engl.* **1997**, *36*, 1342. (d) Lim, J. H.; Lee, H.-J. Lee, K.-B.; Jang, H. G. *Bull. Korean. Chem. Soc.* **1997**, *18*, 1166.

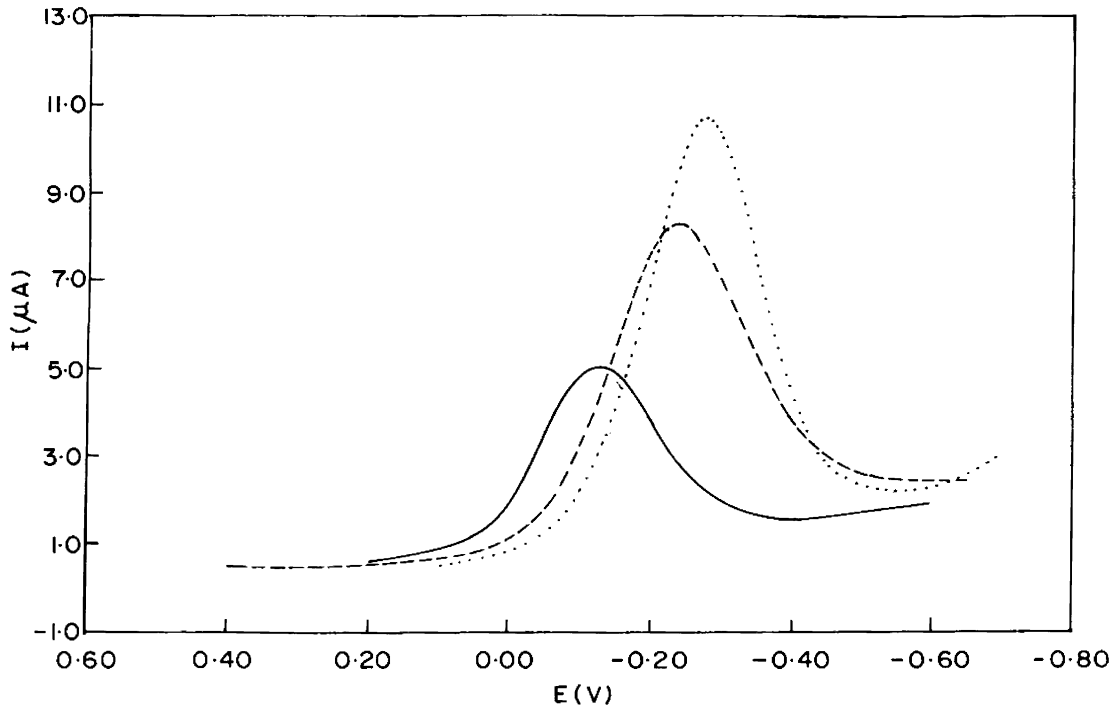

Figure 3. Differential pulse voltammograms of $[Fe(L1)Cl_2]$ (····), $[Fe(L2)Cl_2]$ (- - -), $[Fe(L3)Cl_2]$ (—) in methanol at 25 °C. Complex concentration: 0.001 M. Supporting electrolyte: 0.1 M TBAP. Scan rate 1 mV s^{-1}. Working electrode: Pt sphere. Reference electrode: Ag/Ag^+.

dependence on the nature of the primary ligand,[12−14,33,54] and in fact, the magnitude of the energy of this band represents the Lewis acidity of the iron(III) center as modified by the phenolate ligands. The low energy bands of all the catecholates are shifted to lower energies on replacing the py moiety in [Fe(L1)(DBC)] by the less strongly binding and sterically hindering $-NMe_2$ group as in [Fe(L2)(DBC)] illustrating the importance of steric rather than electronic factors of the phenolate ligands. Similarly, on incorporating the sterically hindering 6-Me substituent as in [Fe(L3)(DBC)] the band is shifted to lower wavelength. Further, on replacing the py moiety in [Fe(L2)(DBC)] by the strongly σ-bonding *N*-methylimidazole moiety to obtain [Fe(L4)(DBC)], the band is shifted[20] to higher energy revealing that electronic effects are critical in catecholate adduct formation.

The position of the low energy catecholate → Fe(III) LMCT band is found to be shifted to higher energies as the substituents[14,55] on the catecholate ring are varied from electron donating to electron withdrawing: H_2DBC (780 nm) > H_2TBC (755 nm) > H_2CAT (725 nm) > H_2TCC (650 nm) for **1**, for example. Electron donating substituents would be expected to raise the energy of the catecholate frontier orbitals and thus minimize the ligand-to-metal energy gap. The similarity between the electronic spectra of the catecholate adducts of the present complexes and the catechol-bound enzymes suggests that the catecholato dianion is chelated to the iron(III) center in the enzymes. Similar spectroscopic characteristics have been observed by Krebs et al.,[55] Que et al. for $[(TPA)Fe^{III}(DBC)]^+$ [15] and $[(NTA)Fe^{III}(DBC)]^{2-}$,[12,14,56]

Table 3. Electrochemical Properties[a] of Fe(III) Complexes in Acetonitrile Solutions

			$E_{1/2}$[b] (V)	
complex	E_{pc} (V)	i_{pc} (μA)	CV[c]	DPV
$[Fe(L1)Cl_2]$	−0.400	29.2	−0.294	−0.297
$[Fe(L2)Cl_2]$	−0.406	24.6	−0.262	−0.266
$[Fe(L3)Cl_2]$	−0.176	17.3	−0.176	−0.152
$[Fe(L4)Cl_2]$	−0.526	17.3	−0.278	−0.280

[a] Measured vs nonaqueous silver reference electrode; add 0.544 V to convert NHE. Scan rate, 50 mV s^{-1}; supporting electrolyte, tetra-*n*-butylammonium perchlorate (0.1 M); complex concentration, 0.001 M. [b] Differential pulse voltammetry (DPV), scan rate, 1 mV s^{-1}; pulse height, 50 mV. [c] $E_{p1/2}$, cathodic potential at half-height.

Kruger et al.[57] for $[(N_4Me_2)Fe^{III}(CAT)]^+$, and Palaniandavar et al.[20,21,58,59] for catechol-bound iron(III) complexes.

Redox Behavior. The electrochemical behavior of the present iron(III) phenolate complexes was studied by employing cyclic voltammetry (CV) and differential pulse voltammetry (DPV) using a stationary platinum sphere as working electrode and a nonaqueous Ag/Ag^+ electrode as reference. In methanol solution, all the complexes exhibit completely irreversible redox behavior with a cathodic wave in the range 0.090−0.258 V (Table 3, Figure 3), but with no anodic wave. For all the complexes, the plots of i_{pc} versus $\nu^{1/2}$ (ν < 0.5 V s^{-1}) are linear, revealing a diffusion controlled redox process. The values of diffusion coefficients (D, 3.4−6.8 × 10^{-6} cm^2/s) were calculated by assuming reversibility

(54) Pyrz, J. W.; Roe, A. L.; Stern, L.; Que, L., Jr. *J. Am. Chem. Soc.* **1985**, *107*, 614.
(55) Duda, M.; Pascaly, M.; Krebs, B. *J. Chem. Soc., Chem. Commun.* **1997**, 835.
(56) White, L. S.; Nilsson,. V.; Pignolet, H.; Que, L., Jr. *J. Am. Chem. Soc.* **1984**, *106*, 8312.
(57) Koch, W. O.; Krüger, H.-J. *Angew. Chem., Int. Ed. Engl.* **1995**, *34*, 2671.
(58) Viswanathan, R.; Palaniandavar, M.; Balasubramanian, T.; Muthiah, T. P. *J. Chem. Soc., Dalton Trans.* **1996**, 2519.
(59) Viswanathan, R.; Palaniandavar, M. *J. Chem. Soc., Dalton Trans.* **1995**, 1259.

Table 4. Kinetic Data[a] for the Catalytic Reaction, Identification of Cleavage Products (see Figure 5), and Their Percent Yield and *m*/*z* Values

complex	intradiol (% yield, *m*/*z*)	extradiol (% yield, *m*/*z*)	other products (% yield, *m*/*z*)	k_{O_2} (M^{-1} s^{-1})
[Fe(L2)Cl_3]	**6** (1.0%, 281)	**8** (0.32%, 224)	**11** (5%, 236), **12** (0.73%, 223), **13** (0.63%, 154)	4.6×10^{-3}
	7 (52.6%, 20.8, 321)	**9**, **10** (0.64%, 208)		
[Fe(L4)Cl_3]	**6** (1.5%, 281)	**9**, **10** (0.1%, 208)	**11** (0.21%, 236)	2.9×10^{-2}
	7 (75.6%, 321)	**7** (75.6%, 321)	**13** (5.64%, 154)	

[a] $k_{O_2} = k_{obs}/[O_2]$. The solubility of O_2 in DMF at 25 °C is 4.86 mM. The kinetic data were obtained by monitoring the disappearance of the lower energy LMCT band.

falls in the range observed for other iron(III) complexes.[58,59] The $E_{1/2}$ values of Fe^{III}/Fe^{II} redox potentials of the present complexes follow the trend **3** > **2** > **4** > **1**, which represents the decrease in Lewis acidity of the iron(III) center, consistent with the above spectral results. On replacing the pyridyl arm in **1** by a $-NMe_2$ group to obtain **2**, the iron(III) center is destabilized due to weak σ-bonding interaction by the sterically demanding $-NMe_2$ group (cf. above). Similarly, on introducing the sterically hindering 6-methyl group on the pyridyl ring in **2** to give **3**, the iron(III) oxidation state is destabilized (cf. above). The Lewis basicity of the *N*-methylimidazole moiety in L4, which is higher than that of the pyridine moiety in L2, leads to enhanced stabilization of the iron(III) oxidation state in **4**, rendering its Fe^{III}/Fe^{II} redox potential more negative. Further, the Fe^{III}/Fe^{II} redox potentials of the present complexes are more negative than that for the [Fe(TPA)Cl_2]Cl complex[20] illustrating that the incorporation of the iron(III)−phenolate bond stabilizes the iron(III) oxidation state.

Catechol 1,2-Dioxygenase Activity of Iron(III) Complexes. The 3,5-di-*tert*-butylcatecholate (DBC^{2-}) adducts were generated in situ in DMF solution, and their reactivity toward O_2 was investigated by monitoring the decay of DBC^{2-}. Interestingly, only **4**·DBC^{2-} and **2**·DBC^{2-} were found to react, and the oxygenation reactions exhibit pseudo-first-order kinetics due to the excess of dioxygen used, as judged from the linearity of the plot of [1 + log(Abs)] versus time (Figure 4). The rates of the reaction (Table 6) were calculated[33,34] by using the equation

$$k_{O_2} = k_{obs}/[O_2]$$

Both GC and GC-MS techniques were used to identify and quantify the oxidative intradiol (**6**, **7**, Table 4, Figure 5) and very small amounts of extradiol (**8**−**10**) and side (**11**−**13**) products of H_2DBC. The products **6** and **7** are derived[13] from the nucleophilic attack of, respectively, Me_2NH as impurity in DMF and piperidine on *cis*,*cis*-muconic anhydride, which is the immediate product of oxidative cleavage.

The very low amounts of the extradiol products are expected because the six-coordinate catecholate adducts of **2** and **4** have no vacant coordination site for O_2 to attack.[60] Since mainly intradiol cleavage products were obtained, the oxidative reactions catalyzed by the complexes correspond exclusively to intradiol-cleavage pathway; hence, the trend in reactivity of **2** and **4** may be illustrated by invoking the novel substrate-activation mechanism proposed[2,15,22,61] for the intradiol-cleaving dioxygenase enzymes. Thus, as previously demonstrated by Que[12,14,15] and Palaniandavar,[20,21,23] the higher Lewis acidity of the iron(III) center in **2** (cf. above) would be expected to confer a higher rate of oxygenation on **2**·DBC^{2-}. But, interestingly, the latter reacts (k_{O_2}, 2.9×10^{-2} M^{-1} s^{-1}) approximately six times slower than **4**·DBC^{2-} does (k_{O_2}, 4.6×10^{-3} M^{-1} s^{-1}), which is consistent with the former displaying a more efficient conversion of the substrate to intradiol products than the latter (**4**: **6**, 1.0; **7**, 52.6%; **2**: **6**, 1.5; **7**, 75.6%). The dissociation of the reaction intermediate into products, which is possibly the rate determining phase of oxygenation reaction as for the enzymes,[2] appears to be facilitated by the more basic *N*-methylimidazole moiety in **4**, leading to the observed higher rate of catechol cleavage. Similar enhancement in rates have been observed by us[23] and Krebs et al.[17] previously.

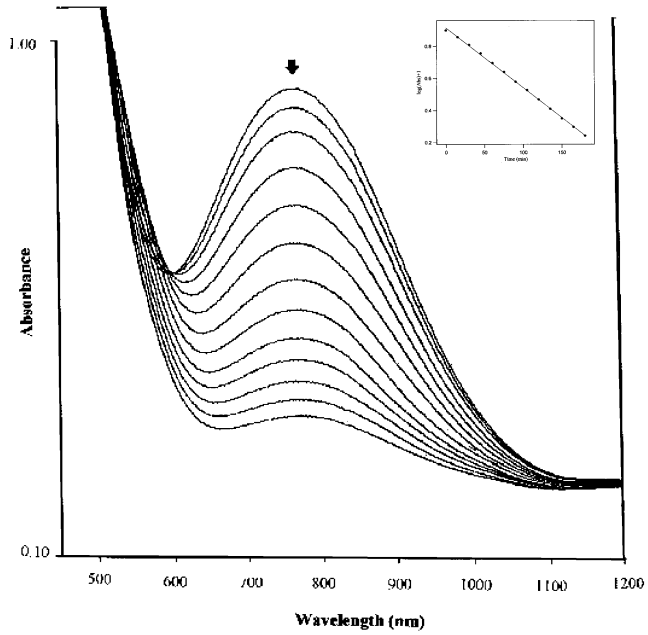

Figure 4. Progress of the reaction of [Fe(L4)(DBC)] with O_2 in DMF solution. The disappearance of the catecholate-to-iron(III) charge-transfer band was monitored. Inset: Plot of [1 + log(Abs)] versus time for the reaction of [Fe(L4)DBC] with O_2 at 25 °C in DMF solution.

The incorporation of a coordinated phenolic hydroxyl group into $[Fe(TPA)(DBC)]^+$ (k_{O_2}, 1.5×10^3 $M^{-1}s^{-1}$)[15] as in [Fe(HDP)(DBC)] [H(HDP) = 2-[(bis(2-pyridylmethyl)-aminomethyl]-4,6-dimethylphenol][12] decreases the Lewis acidity of the iron(III) center and hence lowers the rate of dioxygenation enormously (k_{O_2}, 3.3×10^{-3} M^{-1} s^{-1}). On the other hand, the incorporation of the *p*-nitrophenolate moiety as in **1** leads to a lack of reactivity toward dioxygen and H_2O_2 as well.[18] The *p*-nitrophenolate donor, as it is weakly σ-bonding, does not appear to facilitate the decom-

(60) Jo, D.-H.; Que, L., Jr. *Angew. Chem., Int. Ed.* **2000**, *36*, 4284.
(61) Que, L., Jr.; Lipscomb, J. D.; Munck, E.; Wood, J. M. *Biochim. Biophys. Acta* **1977**, *485*, 60.

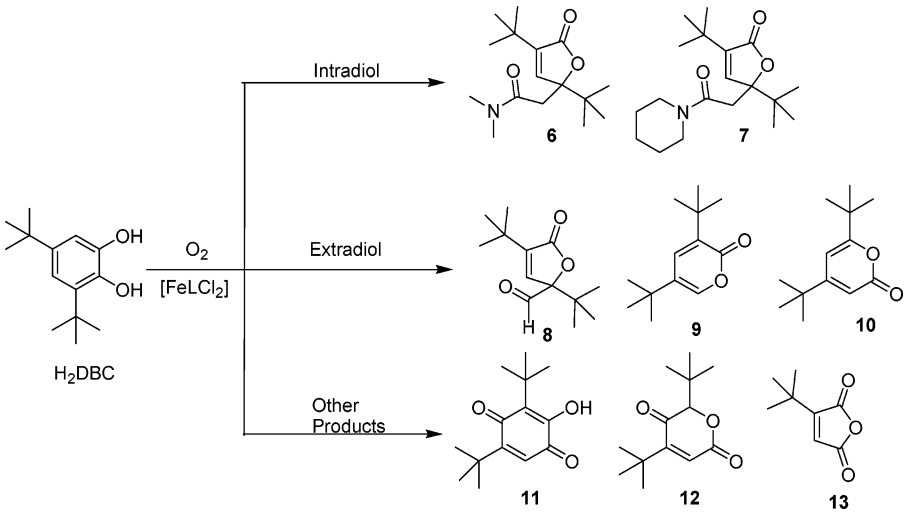

Figure 5. Products of catechol cleavage of 3,5-di-*tert*-butylcatechol (H_2DBC) mediated by [$FeLCl_2$] complexes: 3,5-di-*tert*-butyl-5-(*N*,*N*-dimethylamidomethyl)-2-furanone (**6**), 3,5-di-*tert*-butyl-5-(2-oxo-2-piperidin-1-ylethyl)-5*H*-furan-2-one (**7**), 3,5-di-*tert*-butyl-5-formyl-2-furanone (**8**), 3,5-di-*tert*-butyl-2-pyrone (**9**), 4,6-di-*tert*-butyl-2-pyrone (**10**), 3,5-di-*tert*-butyl-2-hydroxy-1,4-benzoquinone (**11**), 2,5-di-*tert*-butyl-2*H*-pyran-3,6-dione (**12**), 3-*tert*-butylfuran-2,5-dione (**13**).

position of the reaction intermediate into products (cf. above). Also, on replacing one of the pyridyl moieties in **1** by the $-NMe_2$ pendant to obtain **2**, the dioxygenase activity is restored; obviously, the weak coordination of the sterically hindering $-NMe_2$ group (cf. above) enhances the Lewis acidity of the iron(III) center suffciently thereby increasing the reaction rate. Further, on replacing the pendant py moiety in **2** by one more pendant *p*-nitrophenolate moiety to obtain **5** only a slight decrease in reaction rate is observed (k_{O_2}, 3.8×10^{-3} M^{-1} s^{-1}).[23] This is consistent with the presence of *trans*-disposed and significantly different (1.890, 1.993 Å)[23] Fe−O(*p*-nitrophenolate) bonds, which facilitate the unsymmetrical chelation[50] of catecholate and hence the release of products from the reaction intermediate.[13] A similar higher rate of cleavage and higher cleavage yield have been noted, respectively, by Krebs et al.[17] and Palaniandavar et al.[20] for certain bis(phenolate)iron(III) complexes. Furthermore, the inactivity of **3** toward catechol cleavage, despite enhanced Lewis acidity of its iron(III) center, is intriguing. The sterically highly demanding 6-methyl group in this adduct appears to hinder the approach of dioxygen. A similar dioxygenation activity of [Fe(MeTPA)(TPA)Cl_2][16c] [MeTPA = (6-methylpyrid-2-ylmethyl)bis(pyrid-2-ylmethyl)amine] that is extremely lower than that of [Fe(TPA)Cl_2]Cl has been noticed previously. Thus, all the present results reveal the importance of the stereoelectronic properties of coordinated $-NMe_2$ and 6-methylpyridine and *p*-nitrophenolate ligand moieties in fine-tuning the Lewis acidities as well as the rates of dioxygenation. However, the existence of multiple reaction pathways for the small molecule analogues could not be discounted at this stage. So, it is clear that the interplay of several factors, namely, the Lewis acidity, oxygen attack, and release of products from the enzyme−substrate adduct are critically tuned in the enzymes to result in an efficient and facile dioxygenation of the substrate yielding selective cleavage products.

Conclusions and Relevance to Iron Oxygenases

Three new mononuclear iron(III) complexes of tripodal monophenolate ligands offering a N_3O donor set have been isolated and studied as structural, spectral, and functional models for the intradiol-cleaving catechol 1,2-dioxygenase enzymes. In the X-ray crystal structure of one of these complexes, the tripodal ligand is coordinated to the iron(III) center with a distorted octahedral coordination geometry. Interestingly, the Fe−O−C bond angle of 136.1° observed for this complex is higher than the average Fe−O−C bond angle of ∼128.5° reported for other octahedral iron(III)−phenolate complexes. This structural feature, which originates from the other donors of the phenolate ligand, namely, the sterically demanding $-NMe_2$ group, leads to a enhanced rate of catechol cleavage. This is relevant to the stereochemical constraints in the 3,4-PCD enzymes, the function of which is traced to the quite different equatorial and axial Fe−O(tyrosinate) bond distances (1.81, 1.91 Å), as determined by the Fe−O−C bond angles (133°, 148°) and Fe−O−C−C dihedral angles (68°, 24°).[50] The ligand donor functionalities $-NMe_2$, (6-methyl)pyridine, and *N*-methylimidazole exhibit different stereoelectronic effects in clearly influencing the shielding of the iron(III) center and hence its Lewis acidity, as demonstrated by the spectral and electrochemical properties.

The present coordinatively unsaturated iron(III) complexes bind to catecholate substrates without replacing the already bound phenolate or any other donors of the primary ligands. On binding of the catecholates, two new $CAT^{2-} \rightarrow$ Fe(III) LMCT bands appear in the visible region, which is strikingly similar to that observed for the enzyme−substrate complexes in steady state conditions. So, the catecholate adducts containing only one bound phenolate donor are suggested as good synthetic models for an enzyme−substrate complex in which the equatorial but not the axial phenolate is bound to iron(III). The rates of dioxygenase reaction of the complexes could be illustrated not on the basis of the Lewis

acidity of the iron(III) center alone but by assuming that product release is the rate-determining phase of the catalytic reaction, lending support to the electron-transfer mediated substrate activation mechanism proposed by Que and co-workers. Thus, it is remarkable that the imidazole-based complex confers an enhanced reaction rate with efficient conversion of substrate to intradiol cleavage products.

Acknowledgment. We sincerely thank the Department of Science and Technology, New Delhi, for supporting this research [Scheme SR/S1/IC-45/2003 and SP/S1/F-20/2000], and the Council of Scientific and Industrial Research, New Delhi, for a Senior Research Fellowship to M.V. We thank Professor C. N. R. Rao, FRS, and Dr. G. U. Kulkarni, Jawaharlal Nehru Center for Advanced Scientific Research, Bangalore 560 012, India, for kindly providing the diffractometer facility.

Supporting Information Available: Additional tables and figures. This material is available free of charge via the Internet at http://pubs.acs.org.

IC049802B